An experimental approach to study multi-species diseases interactions in wheat using machine learning-aided image analysis.

2024_04_13

Miguel Ángel Corrales Gutiérrez[1], Harleen Kaur[1], Francesca Desiderio[2], Dimitar Kostadinov Douchkov[3], Jiasui Zhan[1], Heriberto Vélëz[1,4,*], Salim Bourras[5*].

Authors affiliation

[1]. Department of Forest Mycology and Plant Pathology, Swedish University of Agricultural Sciences. Almas Allé 5, 75007 Uppsala, Sweden.

[2]. Council for Agricultural Research and Economics (CREA) - Research Centre for Genomics and Bioinformatics, Fiorenzuola d'Arda, Italy

[3]. Leibniz-Institute of Plant Genetics and Crop Plant Research, 06466-Gatersleben, Germany.

[4]. Current address: College of Science, Mathematics and Technology. Wenzhou-Kean University. 88 Daxue Rd, Ouhai, Wenzhou, Zhejiang Province 325060, China.

[5]. Department of Plant Biology, Swedish University of Agricultural Sciences. Almas Allé 5, 75007 Uppsala, Sweden.

Authors for correspondence

Dr. Heriberto Vélëz

hvelez@kean.edu

Prof. Dr. Salim Bourras

salim.bourras@slu.se

Abstract

Fungal plant pathogens causing head blight and leaf blotch diseases are one of the most important threats to cereals such as oat and wheat. Although different resistant varieties have been developed, these diseases are still hard to control thus driving the use of chemical fungicide in Europe and worldwide. Plant breeding programs to develop new varieties with quantitative resistance could result in a longer resistance to the pathogens but require scalable quantitative methods to analyze complex phenotypes. Additionally, in nature, several diseases can occur at the same time due to the coexistence of different pathogen species, thus increasing the genetic complexity of the pathosystem. In the present study we develop a reductionist strategy to study disease resistance at a higher level of organismal complexity, through the application of machine learning to image analysis of artificial pathobiomes. Our results show that such approach enables a meaningful simplification of complex plant multi-pathogen species interactions, allowing the analysis of specific pathogen-pathogen interactions to unravel hidden phenotypic layers that are not visible or quantifiable under field conditions.

Introduction

Wheat is one of the main cultivated crops and a prime source of proteins and carbohydrates in our diets (**de Sousa et al., 2021**). It is cultivated worldwide and is the target of diverse fungal pathogens. Because of its importance to food security, the search for new disease resistance traits has been a major focus for plant pathologists and breeders. Traditionally, we can separate two types of disease resistance: qualitative resistance and quantitative resistance. Qualitative resistance is commonly associated with one, dominant resistance R gene/allele, while quantitative resistance is associated with an assortment of different trait loci (QTLs) representing putative resistance genes with additive effects. Although quantitative resistance is usually less efficient than the strong R gene based qualitative resistance (**Rousseau et al., 2013**), it is generally more durable, effective against a broader spectrum of races of a particular pathogen **(Corwin & Kliebenstein, 2017; McDonald & Linde, 2002; Van den Berg et al., 2014**), and usually involves a higher number of genes. Modern strategies for breeding quantitative disease resistance require the use of extensive genomic and phenotypic data from the host and the pathogen. Additionally, the ability to reveal and properly score complex and diverse phenotypical traits becomes essential to link host/multi-pathogen genotype interactions to their corresponding phenotypes. Such approach which has been coined as 'phenomics', implies the systematic acquisition of high-dimensional data on an organism-wide scale (**Houle *et al*., 2010; Rousseau *et al*., 2013**).

In nature, it is common that different plant pathogens coexist on a single host **(Tollenaere et al., 2016**). Plants have thus developed complex responses to counter act and adapt to complex pathobiomes. This involve a variety of genetic factors rendering breeding for multiple disease resistance (MDR) rather challenging **(Barrett et al., 2021; Orton & Brown, 2016; Wiesner-Hanks & Nelson, 2016**). For example, it has been shown that the biotrophic pathogen *Pseudomonas syringae* induces salicylic-related defense triggering susceptibility of its host to *Alternaria brassicicola*, a necrotrophic pathogen (**Spoel *et al*., 2007**). Also, *Arabidopsis thaliana* plants previously infected with *Albugo candida* show increased susceptibility to an avirulent strain of *Hyaloperonospora arabidopsidis* (**Cooper et al., 2008**). In wheat, primary infection with *Zymoseptoria tritici* can induce systemic susceptibility and systemic shifts in the wheat metabolome and microbiome composition (**Seybold et al., 2020**), but at the same time it can also reduce the incidence of *Puccinia striformis* (**Madariaga, 1986**) or inhibit the sporulation of wheat powdery mildew (**Orton & Brown, 2016**). These findings indicate there are higher levels of genetic organismal complexity regulating host/multi-pathogen interactions.

Such genetic complexity is also highly relevant for so called 'disease complexes' where several pathogen species can act in mixed infections to cause diseases such as ascochyta blight, black spot, and fusarium head blight (FHB). In the latter, over 17 *Fusarium* and non-fusarium species are known to be associated with FHB (**Karlsson et al., 2021**) thus making the disease difficult to control. Species associated with FHB in cereals include *Fusarium graminearum*, *F. langsethiae, F. avenaceum, F. poae, F. culmorum, F. tricinctum, Microdochium majus* and *Microdochium nivale* (**Karlsson et al., 2021**). Broadly speaking, *Fusarium* species can infect cereal hosts in virtually all organs, through the roots, the crown, or the stem base of the plant (**Karlsson et al., 2021**). This complex scenario makes the management of the disease and breeding for resistance particularly challenging considering the variety of tissues and organs that can host pathogenic *Fusarium* species (**Karlsson et al., 2021; Vogelgsang et al., 2008**).

Due to this complex scenario, several types of reductionist resistance screenings have been developed, such as detached leaf assays (**Diamond & Cooke, 1999**), seedling resistance (**Mesterhazy, 1987**), seed germination assay (**Browne & Cooke, 2005**), coleoptiles assay (**Wu et al., 2005**) and response to the *Fusarium* mycotoxin deoxynivalenol (DON) (**Buerstmayr H, Lemmens M, 1996**). All these methods have been useful in the identification of *Fusarium* resistance traits in cereals, and particularly the detached leaf assay, which has been particularly used due to the high correlation between pathogen latent period and quantitative disease resistance in the field (**Diamond & Cooke, 1999; Niks & Skinnes, 1998**). As some pathogenic *Fusarium* species such as *F. avenaceum* or *F. graminearum* can be endophytes in grass plants (**Inch & Gilbert, 2003; Postic *et al*., 2012**), it is relevant to notice that the latent period could be a good predictor of plant resistance due to the well accepted assumption of the endophytic origin of pathogenic *Fusarium* species (**Lofgren et al., 2018**). As a result of this complex scenario (*interactions between pathogens during mixed infections, disease complex with diverse causal agents*), genetic studies of multispecies disease interactions are necessary to gain better understanding of multiple-disease resistance (MDR).

Here we describe a fully featured strategy inspired and co-developed with the Microphenomics platform at the Leibniz-Institute of Plant Genetics and Crop Plant Research (IPK, Germany). This simplified approach enables the study of host/multi-pathogen interactions in a controlled and scalable manner, which is suited for the exploration of large cereal germplasm collections in a space and time-effective manners.

Materials & Methods

Plant growth conditions

An overview of the phenotyping pipeline is provided in **Figure 1**. We used the reference hexaploid wheat cultivars 'Chinese Spring', 'Fielder', and 'Bob White', *Triticum aestivum* spp. *aestivum* parental breeding lines ('Agadir', 'Artico', and 'Victo'), a *T. turgidum* spp. *durum* cultivar ('Latino'), a *T. dicoccum* accession (MG5323), and an old cultivar of *T. turgidum* spp. *turanicum* (Zardak), and commercial spring wheat cultivars were germinated in pots with sterilized substrate at 20-21 °C, RH of 70% and with light intensity of 300 µmol and 18 h light/ 6 h dark photoperiod. Commercial spring wheat cultivars were provided by the Swedish Agricultural Cooperative Lantmännen Lantbruk (Sweden). Plants for inoculation with *Z. tritici* were maintained in a closed infection chamber inside a growth chamber with the same above conditions, and supplemented with and additional LED light sources enriching the light spectrum in the 380 and 700 nM wavelength, respectively (**Supplementary Figure 1**)

Preparation of *Zymoseptoria tritici* inoculum

Z. tritici reference isolates ST99CH_3B8 (3B8), ST99CH_3C4 (3C4), ST99CH_3C7 (3C7), ST99CH_3D5 (3D5), ST99CH_3D7 (3D7), ST99CH_3F2 (3F2), and ST99CH_3G6 (3G6) were isolated in Switzerland in 1999 (courtesy of Prof. Bruce McDonald, ETH Zürich). *Z. tritici* isolates were incubated in yeast extract-malt extract-starch agar, YMS (4 g/L yeast extract, 4 g/L malt extract, 4 g/L sucrose, 16 g/L agar), in darkness at 20 °C for 11 days until the day of the infection. At that stage, spores were collected from the plates by scraping the cells in sterile conditions and resuspendimg them in TWEEN 0.01%. The solution was filtered throughout a sterile filter with pore diameter of 22-25 µm. Spore concentration was calculated with a hemocytometer and adjusted in all isolates to $1x10^6$ spores/ml. Before air gun infection, all isolates were mixed at equal volume and concentration.

Preparation of *Fusarium* sp. inoculum

F. avenaceum, *F. culmorum* and *F. graminearum* were collected from Swedish fields in summer of 2021 and previously genotyped by **Kaur *et al*. (2024)** using universal ITS primers ITS1 (5'-TCCGTAGGTGAACCTGCGG-3') and ITS4 (5'-TCCTCCGCTTATTGATATGC-3'), and species specific primers for *F. graminearum* marker GOFW (5'-ACCTCTGTTGTTCTTCCAGACGG-3') GORV (5'- CTGGTCAGTATTAACCGTGTGTG-3'), and for *F. culmorum* with marker Fc03 (5'-TTCTTGCTAGGGTTGAGGATG-3') Fc02 (5'-GACCTTGACTTTGAGCTTCTTG-3') (**Astrid Bauer & Seigner, 2015; De Biazio *et al*.,**

2008). For coinfections with the three *Fusarium* species, isolates were grown for two weeks at 25 °C on oatmeal agar or OMA (3 g/L ecological oatmeal and 16 g/L agar) and sporulation was induced by incubation under natural light for 3 days. For coinfections with *Zymoseptoria tritici*, all *Fusarium* species were incubated in muesli agar or MA (25 g/L muesli, 2 g/L malt extract and 12 g/L agar) plates at 25 °C for 30 days. After the incubation period, spores were collected by scratching from the plate and suspended in TWEEN 0.01%. The final spore concentration was adjusted to 250 spores/µl and aliquoted into vials at -20 °C until infection day.

Coinfection assays

For coinfections with different *Fusarium* species, 6 cm-length leaf segments were cut from 15-days-old wheat seedlings. Leaf segments were placed with the abaxial surface touching Benzimidazole Agar medium (BA, 5% water agar supplemented with 0.03 mg/L benzimidazole). Three dimensional (3D)-printed frames of polylactic acid (PLA) were designed to keep the leaf surface in contact with the BA medium, thus preventing desiccation of the leaves. A wound was performed in the middle of each leaf segment with a 0.02 mm diameter bore needle, then, a 15 µL drop with a *Fusarium* spore concentration of 10 spores/µl was deposited. Leaf segments were secured with masking tape to seal the wound and avoid curling. As a control, a group of leaf segments were inoculated with TWEEN 0.01%. In the case of *Fusarium* species coinfections, an equal volume and concentration of spores (10 spores/µl) were mixed into a 15 µl drop and inoculated as described above. Pictures were taken at 8 dpi using a DSLR camera. *Fusarium* coinfection assays of the commercial cultivars, lab standards, and parental lines was performed using 4 cm length leaf segments, with a spore concentration of 250 spores/µL and an incubation time of 5 days without frames.

For *F. graminearum* – *Z. tritici* coinfections, 9-days-old wheat seedlings were placed in a closed infection chamber. *Z. tritici* cultures were isolated from YMS plates by scratching and resuspended in TWEEN 0.01%. Spore concentration was calculated with a hemocytometer, and adjusted to 10^6 spores/ml. The different isolates were mixed in equal proportions and sprayed with a spray gun over the seedlings using 0.33 ml per seedling. As a control, a group of plants were inoculated with TWEEN 0.01%. After the inoculation, the chamber was maintained at high humidity (over 70% of RH) and in darkness for 24 hours. Then plants were placed back in a day-night cycle as described above, and kept at high RH by spraying distilled water, using a low-pressure spray gun. Then, 6 cm length leaf segments were cut from *Z. tritici*-infected and mock-inoculated plants at 3-days-post infection (dpi). Secondary infections with

F. graminearum were performed as described above, using a 15 µl drop with a *F. graminearum* spore concentration of 250 sp/µl. Leaf segments were kept on plates with BA medium and maintained in darkness with high RH% for 24 hours, then moved day/night cycle and at high RH until 4 dpi (MG5323) and 5 dpi (Fielder), and then photographed.

Machine learning-aided image analysis

Each leaf segment from the original picture was extracted individually using ImageJ. To quantify disease severity, Jupyter Notebooks (https://jupyter.org/) were used to run code from the PlantCV (https://plantcv.org/) and OpenCV packages (https://opencv.org/). Images showing the juxtaposition of different masks were obtained using the Jupyter Notebooks terminal interface. Bash commands were used to simultaneously analyze multiple samples from one directory, while the PlantCV based script was used to analyze the images and create a JSON file as an output in a selected directory. The implementation of PlantCV allows binary image transformation from original RGB pictures, mask creation, and pixel classification in different predefined classes through a multiclass Naïve Bayes (NB) algorithm. A probability function for red, green, and blue values, allowing pixel classification from these values is calculated. The JSON file output contains the number of counted pixels in each predefined class. Data was transformed to a tabular file and uploaded to the R statistical environment for further analysis.

Statistical analyses

As data did not pass the normality and homoscedasticity tests, a linear model with fixed effects was designed after performing an aligned-rank transformation with the values of necrosis or chlorosis (y) as response variable and cultivar (x_1), zymoseptoria (x_2) and its interaction (x_3) as explanatory variables with their corresponding coefficients ($\beta_1, \beta_2, \beta_3$). The constant µ represents the intercept.

$$y = \mu + \beta_1 x_1 + \beta_2 x_2 + \beta_3 x_3$$

To test statistical differences, we performed an aligned-rank-transformation-two-way-ANOVA (robust two-way-ANOVA) and a *post hoc* test with Tukey adjustment. A Principal Component Analysis (PCA) was carried out with the average value of each cultivar and *Fusarium* combination (each combination has at least 5 biological replicates). Coordinates of each sample in the PCA were extracted to calculate the distance matrix which was used as input for cluster analysis throughout a hierarchical Agglomerative Nesting (AGNES) algorithm.

All statistical analyses were performed with the R statistical software (https://www.r-project.org/, version 4.2.2) in the Rstudio environment (R Core Team, 2022) and the packages: readxl, dplyr, tidyr, stringr, reshape2, ggplot2, multcompView, forcats, ARTool, rcompanion, factoextra, cluster (Graves *et al*., 2023; Kassambara & Mundt, 2020; Kay *et al*., 2021; Maechler *et al*., 2022; Mangiafico, 2023; Wickham, François, *et al*., 2023; Wickham, Vaughan, *et al*., 2023; Wickham, 2007, 2016, 2022, 2023; Wickham & Bryan, 2023).

Results

Phenotypic analysis of leaf segments with single and mixed *Fusarium* sp. infection

We selected plants from the bread wheat cultivar Fielder to perform *Fusarium* infection assays as it turned out it was a good universal susceptible control suitable for obtaining clear disease phenotypes in our hands. Leaf segments were inoculated with *F. avenaceum*, *F. culmorum*, *F. graminearum* and their combinations by drop inoculation (see Material & Methods). PLA frames held the leaf segments in contact with the medium, maintaining the plant tissues humidified and without signs of stress for more than 7 days. Disease symptoms progression on the leaf segments was monitored for one week. At 8 dpi, variability in disease severity between single vs. mixed *Fusarium* sp. infection was scored (**Figure 2**).

We found that *F. graminearum* showed the most severe symptoms, triggering necrosis in large areas of the leaf segment. In contrast, the combination of *F. culmorum* and *F. graminearum* showed the lowest severity of the disease symptoms in comparison with single *F. graminearum* infections. These results suggest that *F. graminearum* is the most aggressive of the three *Fusarium* species tested, and that there are interactions between *F. avenaceum*, *F. culmorum* and *F. graminearum* that could change the plant response. Moreover, we can detect such differences using the detached leaf assay, demonstrating the ability of the image analysis script to distinguish among different phenotypes.

Scoring of *Fusarium* sp. leaf symptoms using image analysis

To define our region of interest (ROI) and reduce the error rate of the algorithm, the picture area inside the PLA frames that hold the leaves was extracted. Then, each leaf segment was extracted as an individual image using a PlantCV based script (Gehan *et al*., 2017). Pixels were manually captured with ImageJ, and their RGB parameters (red, green, blue) were saved in a tab delimited file where we defined each class of pixel. To avoid class imbalance, we collected the same number of pixels for each class (necrosis, chlorosis, healthy tissue, and background).

We thus built a solid training set of over 1000 different pixels from each class. Once the RGB values of each class were defined in a training set, a Naïve Bayes algorithm (Gehan *et al*., 2017) was used to develop a probability function for each pre-defined class. Throughout the probability function, the script classifies each pixel in the different pre-defined classes, creating a binary image for each class that is transformed into a mask. This procedure allows the differentiation of the regions that show necrosis, chlorosis, healthy tissue, or background. Finally, the number of pixels from each class was counted to quantify each feature in every leaf segment (**Figure 3**).

A total of 64 leaf segment pictures were analyzed to test this approach. The results of the quantification of each leaf segment grouped by treatment are illustrated in **Figure 4**. The script correctly identified the infection with *F. graminearum* as the one that triggers the most severe symptoms causing the largest area of necrotic tissue. The level of necrosis observed in the control groups are close to 0, indicating a high performance of the classifier algorithm. We could also quantify previously observed changes that had less necrosis than those infected with *F. graminearum* only. We therefore conclude that the resulting image-segmentation and pixel classification is biologically meaningful, and can correctly differentiate diseases severity levels, and disease symptoms.

Comparison of disease severity values scored visually *vs* with the Naïve Bayes algorithm. We then compared the scorings obtained by a trained person with the results obtained with PlantCV. Usually, the disease severity of *Fusarium* species in detached leaves assays are calculated as a composite phenotype consisting of two attributes: chlorosis and necrosis. The different values of these two variables are combined on a scale from 0 to 5 degrees of severity (**Kaur *et al*. 2024; Supplementary Table 1**). We calculated the percentage of plant pixels classified as necrosis, the percentage of plant pixels classified as chlorosis and the sum of necrosis and chlorosis percentages.

To compare the results obtained by a human with the result of our image analysis, we used an image library previously generated by us (Kaur *et al*., 2024). It consisted of images of detached infection assays with *F. avenaceum*, *F. culmorum*, *F. graminearum* and their combinations using the material described above. Due to the large number of putative comparisons (39 lines and 7 different treatments) and considering the complexity of the data, we decided to perform

an exploratory cluster analysis with the coordinates of each sample obtained from a Principal Component Analysis (PCA) and compare the relative position of each genotype.

We found that the most coherent clustering was obtained with the percentage of necrosis scored with the NB algorithm (**Figure 5, Supplementary Tables 2, 3, 4, 5**). This approximation aggregates the samples in breeding lines (blue), lab standards (pink) and commercial lines (green, red and yellow). Moreover, the clusters obtained with the values of necrosis percentage are similar to the groups obtained with visual scores. In both cases there are two clear groups of commercial lines close to the lab standard and the breeding lines (blue and yellow in manual scoring and orange and yellow in ML scoring). A third commercial line group, which is less similar to the lab standards (green ML scoring), is split in two closely related groups in the manual scoring (green and pink). In contrast, with manual scoring, the parental lines are divided into the cluster of lab standards (Latino, Zardak and MG5323, tetraploid durum wheat) and one of the clusters of commercial lines (Artico, Victo and Agadir, hexaploid wheat). However, beyond these differences, the relative position of each genotype in comparison with the others remains relatively similar. For example, the lab standard Fielder is close to the lines Chinese Spring, Bob White, Eleven, Amulett, and Rogue in both cases, with manual scoring and with necrosis calculated with NB algorithm. In fact, the ML algorithm leads to better separation of the cluster of parental lines (although it aggregates closer tetraploid and hexaploid wheat species), lab standards, and the different commercial lines clusters. These results indicate that our image analysis pipeline can detect small differences in the amount of necrosis, and it suggests that is more accurate quantifying these differences than a discrete scale of disease severity analyzed by the human eye.

To corroborate the existence of differences among *Fusarium* combinations and wheat genotypes, we performed a robust ANOVA analysis (**Supplementary Table 6**), to detect statistically significant differences between genotypes, *Fusarium* combinations, and the combination of both. The results of the ANOVA indicate that there are statistically significative differences ($p<0.01$) between genotypes, *Fusarium* combination, and the combination of both, suggesting that our set up detects specific responses to each Fusarium species in a genotype-specific manner. These results further indicate that our image analysis pipeline is more sensitive to small differences thus allowing us differentiating genotype-specific responses in more coherent clusters. It is noticeable that our results strongly suggest that the manual scoring tends to overestimate the value of necrosis, meanwhile with our image analysis set up we can choose

explicitly if we prioritize to analyze necrosis, chlorosis, or both. Together, our results indicate that our imaging pipeline is accurate and can potentially reveal new layers of information in the analysis of the complex response of the plant to the pathogen.

Phenotypic analysis of mixed *Z. tritici* / *F. graminearum* infections

We decided to test our image analysis set up to process images from coinfections with *F. graminearum*, (the *Fusarium* species which triggers the highest percentage of necrosis), and the hemibiotroph *Z. tritici*. Nine days-old wheat plants were put in control conditions inside the chamber until they were infected with *Z. tritici* spores. The chamber is equipped with an opening that allows infect the plants with an admixture of spores from different *Z. tritici* isolates or a mock solution with an air gun. At 3 dpi, leaf segments were collected from infected and mock plants and inoculated with a suspension of *F. graminearum* spores at a concentration of 10, 100 and 250 spores/µl (see Material & Methods). After an additional 5 days after *F. graminearum* infection we took pictures of the leaf segments, and we analyzed the levels of necrosis and chlorosis using our pipeline (**Figure 6A**). The NB algorithm recognized higher levels of necrosis and chlorosis in leaf segments infected at a concentration of 10 spores/µl in comparison with the negative controls, although the differences are not consistent enough to be statistically significant (**Figure 6B**). Leaf segments inoculated with a concentration of 100 and 250 spores/µl showed similar levels of necrosis and chlorosis, although leaf segments inoculated at 250 spores/µl tend to have more severe disease symptoms (**Figure 6B, 6C**). Interestingly, differences in necrotic and chlorotic areas between leaf segments from *Z. tritici* infected plants and mock plants are detected by the NB algorithm, indicating an effect of primary infection with *Z. tritici* on secondary infection with *F. graminearum*.

Finally, we further assessed the performance of the set up in two different wheat cultivars. We developed a similar coinfection assay, evaluating disease severity symptom in 4 dpi (accession MG5323, tetraploid wheat) or 5 dpi (cv. Fielder, hexaploid wheat) after *F. graminearum* inoculation. Consistent with previous results, the image analysis reveals differences that are clear throughout visual inspection of the leaf segments (**Figure 7A**). Accession MG5323 seems less resistant to *F. graminearum* in comparison to Fielder (**Figure 7B**). Moreover, our pipeline can detect a trend in *Z. tritici* infected Fielder plants to develop less necrosis in comparison with mock plants, although this difference is not statistically significant. Additionally, even though we cannot detect differences in the chlorotic area between mock and *Z. tritici* infected Fielder plants, neither visually nor with our pipeline, our set up still detects an inhibition of the

chlorotic area in *Z. tritici* infected MG5323 plants in comparison with mock. In fact, this difference is statistically significant and can be confirmed visually.

Together, these results suggest that *Z. tritici* infection can modify the host response to *F. graminearum*. This modulation seems to depend on the wheat genotype/specie (tetraploid or hexaploid). In fact, this is coherent with our results from *Fusarium* coinfections, as we can group genotypes by their specific response to each *Fusarium* combination. Besides, our results indicate that our pipeline can detect disease interactions throughout changes in the phenotype. Moreover, the NB algorithm has detected changes related with *Z. tritici* infection in the necrosis, relatively easy to assess visually, and in the chlorosis, a difficult phenotypical trait to measure, allowing us to catch these changes in the plant response to *F. graminearum*. It means, our set up seems to allow a meticulous and objective analysis of the phenotypical responses of wheat to different pathogens and pathogen combinations.

Discussion

Experimental set up

In this study we present an original set up allowing the study of disease interactions in wheat. The detached leaf assay is highly suitable for large scale screens due to the relatively short time from seed to inoculation, and the low requirements of space. In fact, the full procedure can be performed in 17 days facilitating the screening of large populations. Another advantage of the system is the increased consistency between replicates, particularly when using our chamber where the air is saturated with *Z. tritici* spores during the infection. As with other systems, our strategy has also some limitations, and the predictive power of such approach must be carefully evaluated in a pathosystem-specific manner. However, it has been demonstrated that detached leaf assays can be used to predict resistance traits, thus giving us confidence that our strategy is suitable for resistance screenings (Diamond & Cooke, 1999; Niks & Skinnes, 1998).

Image analysis strategy

Currently, advances in computer sciences and machine learning algorithms have enabled the use high-throughput imaging to analyze disease symptoms in a quantitative manner (Bohnenkamp *et al*., 2021; Gehan *et al*., 2017; Karisto *et al*., 2018; Rousseau *et al*., 2013; Shoaib *et al*., 2022; Stewart *et al*., 2016; Stewart & McDonald, 2014). Here, we present the application of one of these machine learning algorithms, Naïve Bayes, to the detection and quantification of phenotypical differences in disease severity. The image analysis set up based

on the PlantCV package allows us to detect and quantify these differences. The algorithm has been demonstrated to be robust enough to analyze pictures with different parameters of exposition time and lens aperture. Moreover, this strategy facilitates an objective quantification of the disease symptom severity. There are several advantages of our pipeline in comparison with previous pipelines (Laflamme *et al*., 2016; Peressotti *et al*., 2011; Perochon & Doohan, 2016). This includes for example the possibility of normalizing the disease area to the total area of the leave, the possibility to analyzed complex, multilayered phenotype (necrosis and chlorosis), and the capacity of parallelize the script and automatize the extraction of data from large datasets.

Additionally, our results show that the image analysis can detect differences in the necrotic area in early stages of the infection (4 dpi) even at low spore concentration (10 spores/µl), demonstrating that our set up is highly sensitive. Although it seems that the percentage of necrosis is the most similar characteristic in the manual disease scoring, we cannot exclude the percentage of chlorosis as another valuable phenotype. Necrosis usually appears in the leaf as a dark lesion. This characteristic color, well differentiated from the green of the leaf, facilitates the training of the algorithm. Chlorosis, however, lays near the yellow color, which is adjacent to the green in the visible spectrum, plus it could also be triggered abiotic stress. This is especially relevant as chlorosis is a disease symptom which is difficult to quantify and can give us valuable clues about changes at molecular level in pathogen-host interactions.

Statistical observations and their meaning

We have performed a robust ANOVA over our linear model as our data did not pass normality tests. As we did not obtain a high enough number of samples, even in the case the data follows the assumptions of normality and homoscedasticity the small size of the population would make the data sensitive to bias due to outliers and influential points, making it almost impossible to pass the tests. In any case, differences are robust enough to be significative with parametric and non-parametric methods, suggesting that our analysis pipeline can detect differences that could be biologically meaningful.

Although *F. graminearum* and *F. culmorum* seem to be more aggressive than *F. avenaceum*, still, each genotype has a typical response for each pathogen and pathogen combination, indicating that there are specific interactions between cultivars and pathogens. This is especially evident as we can aggregate cultivars in clusters depending on their specific

412 responses to each pathogen and pathogen combination. The clustering analysis of the PCA
413 coordinates also reveals patterns in the data collected manually and by the NB algorithm. There
414 are several tools to analyze putative clusters such as K-means clustering or model-based
415 clustering, but Hierarchical Clustering is a standard in this type of analysis with a relatively
416 low computational requirement. AGNES is one of the most commons Hierarchical Clustering
417 algorithms but has disadvantages as it is sensitive to outliers. Despite this, the clustering is
418 coherent with our data, showing that manual scoring and ML scoring are similar. In fact,
419 clusters based on ML scoring are more consistent, suggesting an increased accuracy of the
420 algorithm.
421
422 **Biological relevance**
423 Our results show that *F. graminearum* induced the highest levels of necrosis in leaves in
424 comparison to *F. avenaceum* and *F. culmorum*. Interestingly, different combinations of
425 *Fusarium* species trigger specific different responses in the host. We found a statistical
426 difference between single *F. graminearum* infections compared with *F. culmorum* and *F.*
427 *graminearum* combined, where the latter developing less necrotic areas than *F. gramineaurm*
428 alone. Despite the small populations size, our results strongly support the hypothesis that
429 *Fusarium* species do interact in a way that changes the host response. This idea is especially
430 relevant as FHB is a disease with different, interacting, causal agents. Similarly, *Z. tritici* - *F.*
431 *graminearum* coinfections also reveal that pathogen-pathogen interactions are measurable and
432 genotype-specific manner, which we argue is an important observation suggesting that traits
433 controlling MDR could be genetically mapped using mixed infection strategies.
434

Supplementary Material

Supplementary figures

Supplementary Figure 1. Infection chamber used for *Z. tritici* inoculations of wheat seedlings.

Supplementary tables

Supplementary Table 1. Disease severity score index.

Supplementary Table 2. Cluster composition based on manual scoring of disease severity from Figure 5A.

Supplementary Table 3. Cluster composition based on naïve bayes scoring of 'necrosis' from Figure 5B.

Supplementary Table 4. Cluster composition based on naïve bayes scoring of 'chlorosis' from Figure 5C.

Supplementary Table 5. Cluster composition based on naïve bayes scoring of 'necrosis + chlorosis' from Figure 5D.

Supplementary Table 6. ANOVA performed with disease symptom quantification obtained with our machine learning based set up.

Supplementary files

Supplementary File 1. G-code for the 3D printed PLA frames used to keep the leaf segments in contact with the agar medium.

Supplementary File 2. Jupyter Notebook containing the scripts to analyze pictures with the naïve bayes algorithm.

Supplementary File 3. Numerical data underlying the statistical analysis of Figures 2, 5, 6 and 7.

Supplementary File 4. Html file with the R scripts underlying all the analyses showed in the figures.

Data availability

GitHub DOI. 10.5281/zenodo.10697381

Funding

This was supported by funding from the Swedish Research Council for Sustainable Development FORMAS (grant number 2020-01007) and the Carl Trygger Foundation (grant number 21:1171).

Aknowledgment

We would like to acknowledge Fredric Hedlund and Ayano Tanaka for technical assistance with the growth facilities at SLU Biocentrum. We would also like to acknowledge the support of the Plant Protection Extensions 'Växtskyddscentralerna' of the Swedish Board of Agriculture 'Jordbruksverket' (https://jordbruksverket.se/) with the acquisition of field isolates. We also thank Katarina Ihrmark and Maria Jonsson for their technical assistance.

References

Astrid Bauer, R. S., & Seigner, L. (2015). Detection, Identification and Quantification of Fusarium graminearum and Fusarium culmorum in Wheat Kernels by PCR Techniques. *Journal of Plant Pathology & Microbiology*, *06*(07). https://doi.org/10.4172/2157-7471.1000287

Barrett, L. G., Zala, M., Mikaberidze, A., Alassimone, J., Ahmad, M., McDonald, B. A., & Sánchez-Vallet, A. (2021). Mixed infections alter transmission potential in a fungal plant pathogen. *Environmental Microbiology*, *23*(4), 2315–2330. https://doi.org/10.1111/1462-2920.15417

Bohnenkamp, D., Behmann, J., Paulus, S., Steiner, U., & Mahlein, A. K. (2021). A Hyperspectral Library of Foliar Diseases of Wheat. *Phytopathology*, *111*(9), 1583–1593. https://doi.org/10.1094/PHYTO-09-19-0335-R

Browne, R. A., & Cooke, B. M. (2005). Resistance of wheat to Fusarium spp. in an in vitro seed germination assay and preliminary investigations into the relationship with Fusarium head blight resistance. *Euphytica*, *141*(1–2), 23–32. https://doi.org/10.1007/s10681-005-4820-0

Buerstmayr H, Lemmens M, G. H. and R. P. (1996). Breeding for scab resistance in wheat: Inheritance of resistance and possibilities for in vitro selection. *Proceedings of the Workshop on Fusarium Head Scab: Global Status and Future Prospects*, 52–58.

Cooper, A. J., Latunde-Dada, A. O., Woods-Tör, A., Lynn, J., Lucas, J. A., Crute, I. R., & Holub, E. B. (2008). Basic compatibility of Albugo candida in Arabidopsis thaliana and Brassica juncea causes broad-spectrum suppression of innate immunity. *Molecular Plant-Microbe Interactions*, *21*(6), 745–756. https://doi.org/10.1094/MPMI-21-6-0745

Corwin, J. A., & Kliebenstein, D. J. (2017). Quantitative resistance: More than just perception of a pathogen. *Plant Cell*, *29*(4), 655–665. https://doi.org/10.1105/tpc.16.00915

De Biazio, G. R., Leite, G. G. S., Tessmann, D. J., & Barbosa-Tessmann, I. P. (2008). A new PCR approach for the identification of Fusarium graminearum. *Brazilian Journal of Microbiology*, *39*(3), 554–560. https://doi.org/10.1590/s1517-83822008000300028

de Sousa, T., Ribeiro, M., Sabença, C., & Igrejas, G. (2021). The 10,000-year success story of wheat! In *Foods* (Vol. 10, Issue 9). MDPI. https://doi.org/10.3390/foods10092124

Dean, R., Van Kan, J. A. L., Pretorius, Z. A., Hammond-Kosack, K. E., Di Pietro, A., Spanu, P. D., Rudd, J. J., Dickman, M., Kahmann, R., Ellis, J., & Foster, G. D. (2012). The Top 10 fungal pathogens in molecular plant pathology. *Molecular Plant Pathology*, *13*(4),

414–430. https://doi.org/10.1111/j.1364-3703.2011.00783.x

Diamond, H., & Cooke, B. M. (1999). Towards the development of a novel in vitro strategy for early screening of Fusarium Ear Blight resistance in adult winter wheat plants. *Pest Management Focus*, *5*(1), 2.

Fagundes, W. C., Haueisen, J., & Stukenbrock, E. H. (2020). Dissecting the Biology of the Fungal Wheat Pathogen Zymoseptoria tritici: A Laboratory Workflow. *Current Protocols in Microbiology*, *59*(1), 1–27. https://doi.org/10.1002/cpmc.128

Gehan, M. A., Fahlgren, N., Abbasi, A., Berry, J. C., Callen, S. T., Chavez, L., Doust, A. N., Feldman, M. J., Gilbert, K. B., Hodge, J. G., Hoyer, J. S., Lin, A., Liu, S., Lizárraga, C., Lorence, A., Miller, M., Platon, E., Tessman, M., & Sax, T. (2017). PlantCV v2: Image analysis software for high-throughput plant phenotyping. *PeerJ*, *2017*(12), 1–23. https://doi.org/10.7717/peerj.4088

Graves, S., Piepho, H.-P., & with help from Sundar Dorai-Raj, L. S. (2023). *multcompView: Visualizations of Paired Comparisons*. https://cran.r-project.org/package=multcompView

Houle, D., Govindaraju, D. R., & Omholt, S. (2010). Phenomics: The next challenge. *Nature Reviews Genetics*, *11*(12), 855–866. https://doi.org/10.1038/nrg2897

Inch, S., & Gilbert, J. (2003). The incidence of Fusarium species recovered from inflorescences of wild grasses in southern Manitoba. *Canadian Journal of Plant Pathology*, *25*(4), 379–383. https://doi.org/10.1080/07060660309507093

Karisto, P., Hund, A., Yu, K., Anderegg, J., Walter, A., Mascher, F., McDonald, B. A., & Mikaberidze, A. (2018). Ranking quantitative resistance to septoria tritici blotch in elite wheat cultivars using automated image analysis. *Phytopathology*, *108*(5), 568–581. https://doi.org/10.1094/PHYTO-04-17-0163-R

Karlsson, I., Persson, P., & Friberg, H. (2021). Fusarium Head Blight From a Microbiome Perspective. *Frontiers in Microbiology*, *12*(March), 1–17. https://doi.org/10.3389/fmicb.2021.628373

Kassambara, A., & Mundt, F. (2020). *factoextra: Extract and Visualize the Results of Multivariate Data Analyses*. https://cran.r-project.org/package=factoextra

Kaur, H., Vilvert, E., Corrales Gutiérrez, M. Á., Zhan, J., Douchkov, D., Desiderio, F., Vélëz, H., & Salim, B. (2024). Survey of the wheat mycobiome associated with leaf blotch and head blight diseases in Sweden. *BiorXiv*.

Kay, M., Elkin, L. A., Higgins, J. J., & Wobbrock, J. O. (2021). *{ARTool}: Aligned Rank Transform for Nonparametric Factorial ANOVAs*.

https://doi.org/10.5281/zenodo.594511

Laflamme, B., Middleton, M., Lo, T., Desveaux, D., & Guttman, D. S. (2016). Image-based quantification of plant immunity and disease. *Molecular Plant-Microbe Interactions*, *29*(12), 919–924. https://doi.org/10.1094/MPMI-07-16-0129-TA

Lofgren, L. A., LeBlanc, N. R., Certano, A. K., Nachtigall, J., LaBine, K. M., Riddle, J., Broz, K., Dong, Y., Bethan, B., Kafer, C. W., & Kistler, H. C. (2018). Fusarium graminearum: pathogen or endophyte of North American grasses? *New Phytologist*, *217*(3), 1203–1212. https://doi.org/10.1111/nph.14894

Madariaga, R. (1986). Interactions of Puccinia striiformis and Mycosphaerella graminicola on Wheat . *Plant Disease*, *70*(7), 651. https://doi.org/10.1094/pd-70-651

Maechler, M., Rousseeuw, P., Struyf, A., Hubert, M., & Hornik, K. (2022). *cluster: Cluster Analysis Basics and Extensions*. https://cran.r-project.org/package=cluster

Mangiafico, S. S. (2023). *{rcompanion}: Functions to Support Extension Education Program Evaluation*. https://cran.r-project.org/package=rcompanion/

McDonald, B. A., & Linde, C. (2002). Pathogen population genetics, evolutionary potential, and durable resistance. *Annual Review of Phytopathology*, *40*, 349–379. https://doi.org/10.1146/annurev.phyto.40.120501.101443

Mesterhazy, A. (1987). Selection of Head Blight Resistant Wheats Through Improved Seedling Resistance. *Plant Breeding*, *98*(1), 25–36. https://doi.org/10.1111/j.1439-0523.1987.tb01086.x

Niks, R., & Skinnes, H. (1998). Partial resistance. In B. Cooke (Ed.), *Airbone pathogens on cereals*. Office for Official Publications of the European Communities.

Orton, E. S., & Brown, J. K. M. (2016). Reduction of growth and reproduction of the biotrophic fungus Blumeria graminis in the presence of a necrotrophic pathogen. *Frontiers in Plant Science*, *7*(MAY2016). https://doi.org/10.3389/fpls.2016.00742

Peressotti, E., Duchêne, E., Merdinoglu, D., & Mestre, P. (2011). A semi-automatic non-destructive method to quantify grapevine downy mildew sporulation. *Journal of Microbiological Methods*, *84*(2), 265–271. https://doi.org/10.1016/j.mimet.2010.12.009

Perochon, A., & Doohan, F. (2016). Assessment of Wheat Resistance to Fusarium graminearum by Automated Image Analysis of Detached Leaves Assay. *Bio-Protocol*, *6*(24), 2–8. https://doi.org/10.21769/bioprotoc.2065

Postic, J., Cosic, J., Vrandecic, K., Jurkovic, D., Saleh, A. A., & Leslie, J. F. (2012). Diversity of Fusarium species isolated from weeds and plant debris in Croatia. *Journal of Phytopathology*, *160*(2), 76–81. https://doi.org/10.1111/j.1439-0434.2011.01863.x

R Core Team. (2022). *R: A Language and Environment for Statistical Computing*. https://www.r-project.org/

Rousseau, C., Belin, E., Bove, E., Rousseau, D., Fabre, F., Berruyer, R., Guillaumès, J., Manceau, C., Jacques, M. A., & Boureau, T. (2013). High throughput quantitative phenotyping of plant resistance using chlorophyll fluorescence image analysis. *Plant Methods*, *9*(1), 1–13. https://doi.org/10.1186/1746-4811-9-17

Seybold, H., Demetrowitsch, T. J., Hassani, M. A., Szymczak, S., Reim, E., Haueisen, J., Lübbers, L., Rühlemann, M., Franke, A., Schwarz, K., & Stukenbrock, E. H. (2020). A fungal pathogen induces systemic susceptibility and systemic shifts in wheat metabolome and microbiome composition. *Nature Communications*, *11*(1), 1–12. https://doi.org/10.1038/s41467-020-15633-x

Shoaib, M., Shah, B., Hussain, T., Ali, A., Ullah, A., Alenezi, F., Gechev, T., Ali, F., & Syed, I. (2022). A deep learning-based model for plant lesion segmentation, subtype identification, and survival probability estimation. *Frontiers in Plant Science*, *13*(December), 1–15. https://doi.org/10.3389/fpls.2022.1095547

Spoel, S. H., Johnson, J. S., & Dong, X. (2007). Regulation of tradeoffs between plant defenses against pathogens with different lifestyles. *Proceedings of the National Academy of Sciences of the United States of America*, *104*(47), 18842–18847. https://doi.org/10.1073/pnas.0708139104

Stewart, E. L., Hagerty, C. H., Mikaberidze, A., Mundt, C. C., Zhong, Z., & McDonald, B. A. (2016). An improved method for measuring quantitative resistance to the wheat pathogen Zymoseptoria tritici using high-throughput automated image analysis. *Phytopathology*, *106*(7), 782–788. https://doi.org/10.1094/PHYTO-01-16-0018-R

Stewart, E. L., & McDonald, B. A. (2014). Measuring quantitative virulence in the wheat pathogen zymoseptoria tritici using high-throughput automated image analysis. *Phytopathology*, *104*(9), 985–992. https://doi.org/10.1094/PHYTO-11-13-0328-R

Tollenaere, C., Susi, H., & Laine, A. L. (2016). Evolutionary and Epidemiological Implications of Multiple Infection in Plants. *Trends in Plant Science*, *21*(1), 80–90. https://doi.org/10.1016/j.tplants.2015.10.014

Van den Berg, F., Lannou, C., Gilligan, C. A., & Van den Bosch, F. (2014). Quantitative resistance can lead to evolutionary changes in traits not targeted by the resistance QTLs. *Evolutionary Applications*, *7*(3), 370–380. https://doi.org/10.1111/eva.12130

Vogelgsang, S., Sulyok, M., Hecker, A., Jenny, E., Krska, R., Schuhmacher, R., & Forrer, H. R. (2008). Toxigenicity and pathogenicity of Fusarium poae and Fusarium avenaceum

615 on wheat. *European Journal of Plant Pathology*, *122*(2), 265–276.
616 https://doi.org/10.1007/s10658-008-9279-0
617 Wickham, H. (2007). Reshaping Data with the {reshape} Package. *Journal of Statistical*
618 *Software*, *21*(12), 1–20. http://www.jstatsoft.org/v21/i12/
619 Wickham, H. (2016). *ggplot2: Elegant Graphics for Data Analysis*. Springer-Verlag New
620 York. https://ggplot2.tidyverse.org
621 Wickham, H. (2022). *stringr: Simple, Consistent Wrappers for Common String Operations*.
622 https://cran.r-project.org/package=stringr
623 Wickham, H. (2023). *forcats: Tools for Working with Categorical Variables (Factors)*.
624 https://cran.r-project.org/package=forcats
625 Wickham, H., & Bryan, J. (2023). *readxl: Read Excel Files*. https://cran.r-
626 project.org/package=readxl
627 Wickham, H., François, R., Henry, L., Müller, K., & Vaughan, D. (2023). *dplyr: A Grammar*
628 *of Data Manipulation*. https://cran.r-project.org/package=dplyr
629 Wickham, H., Vaughan, D., & Girlich, M. (2023). *tidyr: Tidy Messy Data*. https://cran.r-
630 project.org/package=tidyr
631 Wiesner-Hanks, T., & Nelson, R. (2016). Multiple Disease Resistance in Plants. *Annual*
632 *Review of Phytopathology*, *54*, 229–252. https://doi.org/10.1146/annurev-phyto-080615-
633 100037
634 Wu, A. B., Li, H. P., Zhao, C. S., & Liao, Y. C. (2005). Comparative pathogenicity of
635 Fusarium graminearum isolates from China revealed by wheat coleoptile and floret
636 inoculations. *Mycopathologia*, *160*(1), 75–83. https://doi.org/10.1007/s11046-005-1153-
637 4
638

639 **Figures**

640

641

642

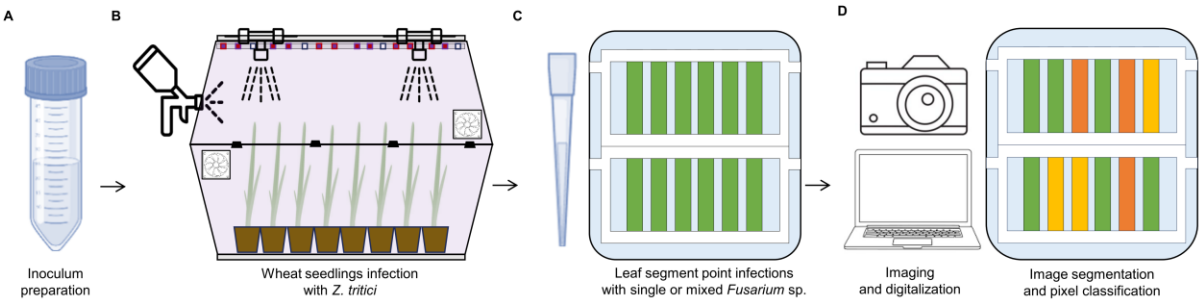

643

644 **Figure 1**. Generic overview of the phenotyping pipeline.

645 **(A)** Step 1: 11-days-old *Z. tritici* (an hemibiotroph) culture is scratched from YMS plates, resuspended
646 in TWEEN 0.01% **(B)** Step 2: wheat seedlings are inoculated with *Z. tritici* and kept in a closed infection
647 chamber kept until the appropriate stage. **(C)** Step 3: after 3 days, leaf fragments are harvested,
648 mounted on agar plates. and infected with a spore suspension of *Fusarium* spp. **(D)** Step 4: after 4-7
649 days of incubation, pictures of the disease symptoms were taken with a DSLR camera. The pictures
650 were analyzed with a combination of ImageJ, PlantCV python scripts, and R statistical software.5

651

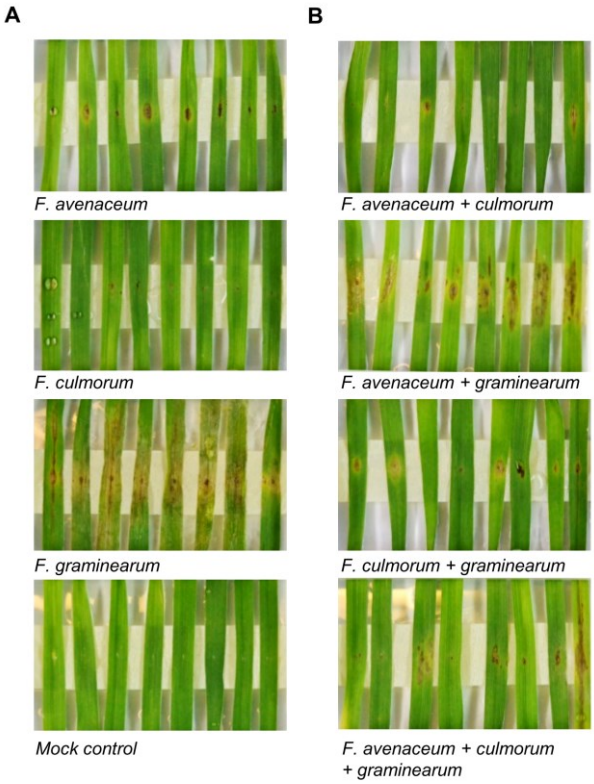

Figure 2. Infection of wheat leaf segments with single and mixed *Fusarium* sp. The cultivar Fielder was inoculated with *F. avenaceum*, *F. culmorum* and *F. graminearum* isolates from Sweden. Pictures were taken at 8 dpi. Two independent experiments with 8 biological replicates per treatment we performed.

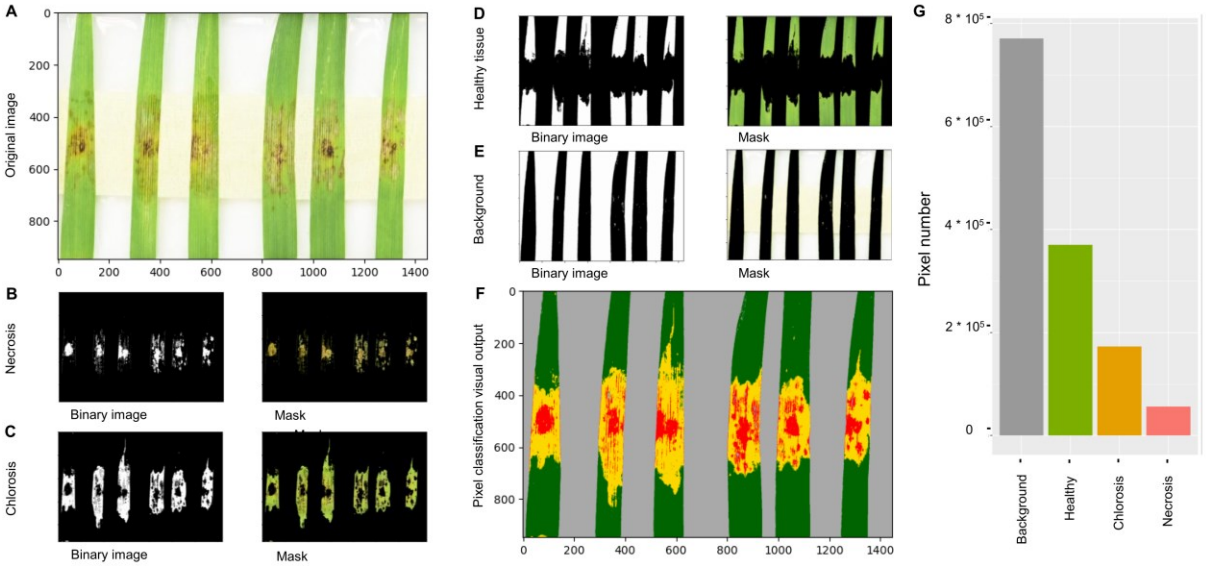

Figure 3. Analysis of disease symptoms using image segmentation and pixel classification. **(A)** Unprocessed images of symptoms caused by *F. greaminearum* on wheat leaves **(B-E)** NB image segmentation and pixel classification of tissue types into **(B)** necrosis, **(C)** chlorosis, **(D)** healthy tissue, and finally **(D)** background. **(F)** Visualization and reconstruction of the original image using pre-defined pseudo colors classes for necrosis (red), chlorosis (yellow), healthy tissue (green), and background (gray). **(G)** Quantification of the pixel areas from the image in (F) and visualization as a bar plot.

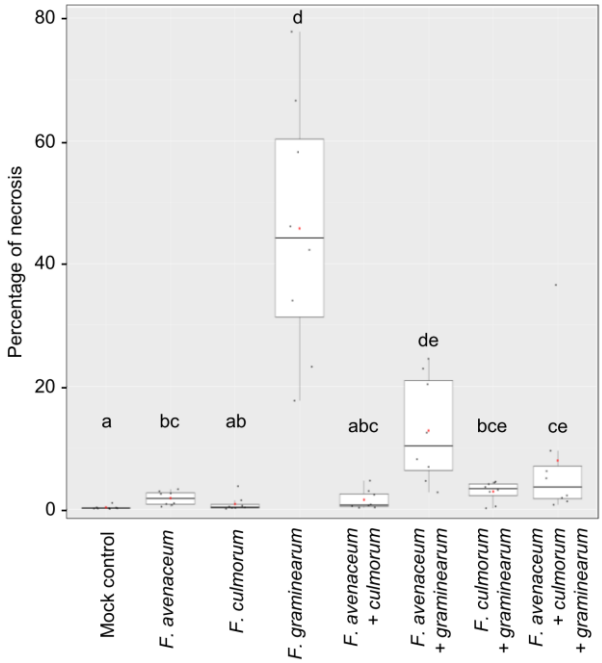

668

669

670 **Figure 4**. Quantification of disease severity using the Naïve Bayes algorithm.

671 Pictures from Figure 2 were analyzed using the pipeline described in Figure 3. The percentage of pixel

672 area corresponding to 'necrosis' as described in Figure 3 was calculated. Statistically significant group

673 are indicated with a letter code a-e (two-way robust ANOVA: $p < 0.05$)

674

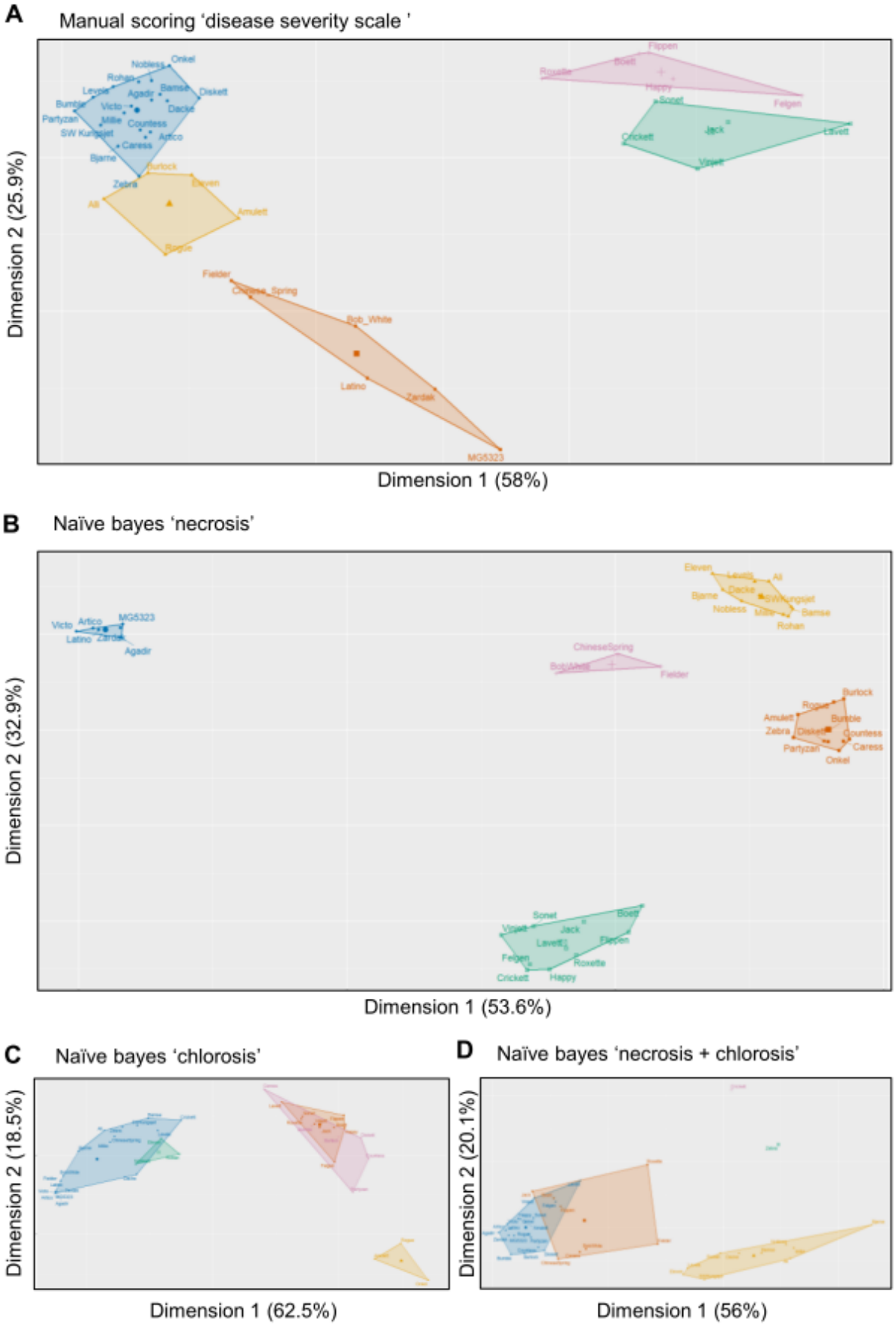

675

676

677

678 **Figure 5**. Cluster analysis of genotype responses to infections with single and mixed *Fusarium species*
679 **(A)** Cluster obtained from manual scoring of the symptoms. Cluster derived from NB analysis of the
680 phenotypic classes **(B)** for 'necrosis', **(C)** for 'chlorosis', and **(D)** for 'necrosis' and 'chlorosis' combined.
681 The Agglomerative nesting (AGNES) algorithm was applied to the distance matrix of the mean value of
682 the PCA coordinates of each sample to develop the dendrogram. The defined number of clusters is 5
683 (k = 5). The exact content of each cluster is provided in Supplementary Tables 2, 3, 4, and 5.

684

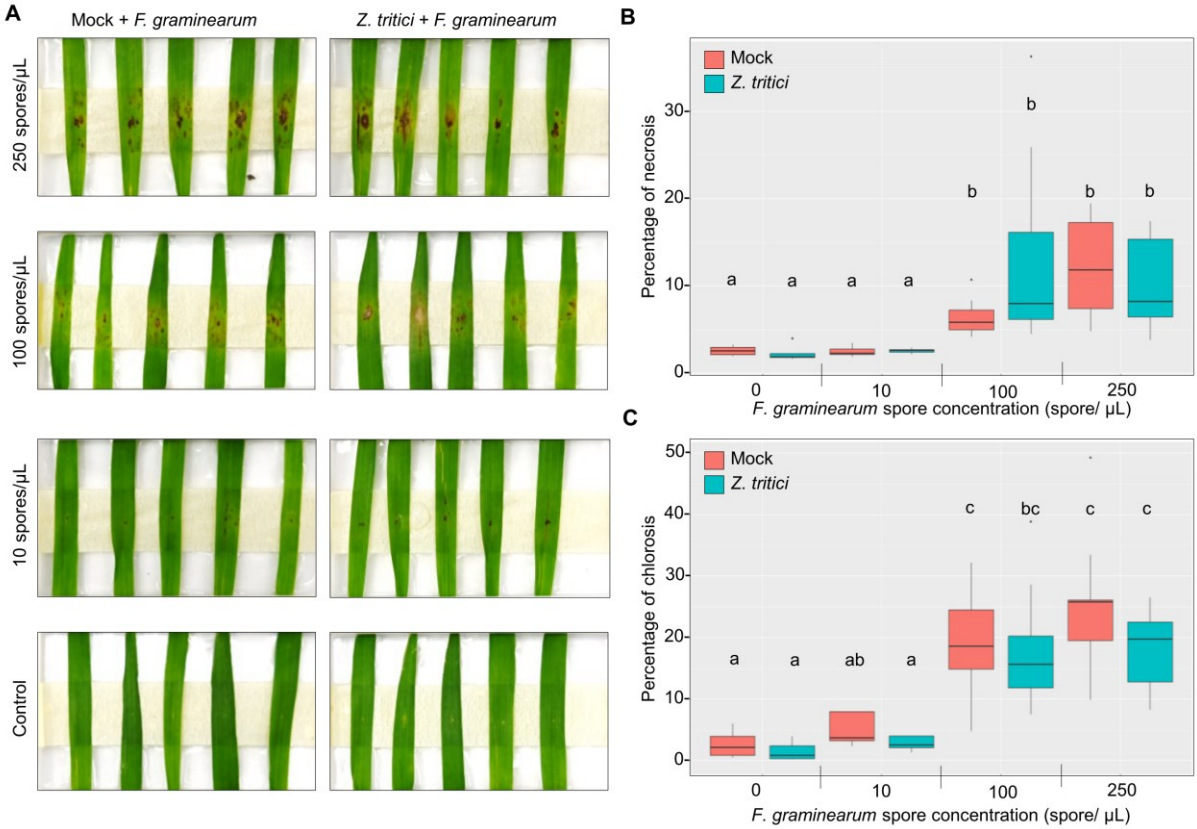

Figure 6. Dose-dependent *F. graminearum* symptom severity in coinfections assays with *Z. tritici* **(A)** Original pictures from one experiment with 5 biological replicates applied to our image analysis pipeline. **(B)** Soring of the percentage necrosis using the NB algorithm. **(C)** Scoring of the percentage of chlorosis using the NB algorithm. In (B-C) control treatment where primary infection with *Z. tritici* was replaced by Mock are indicated in 'red'. Treatments where plants were coinfected with *Z. tritici* and *F. graminearum* are indicated in 'blue'. The letters a-b refer to two groups of treatments with statistically significant differences (two-way robust ANOVA: $p < 0.05$).

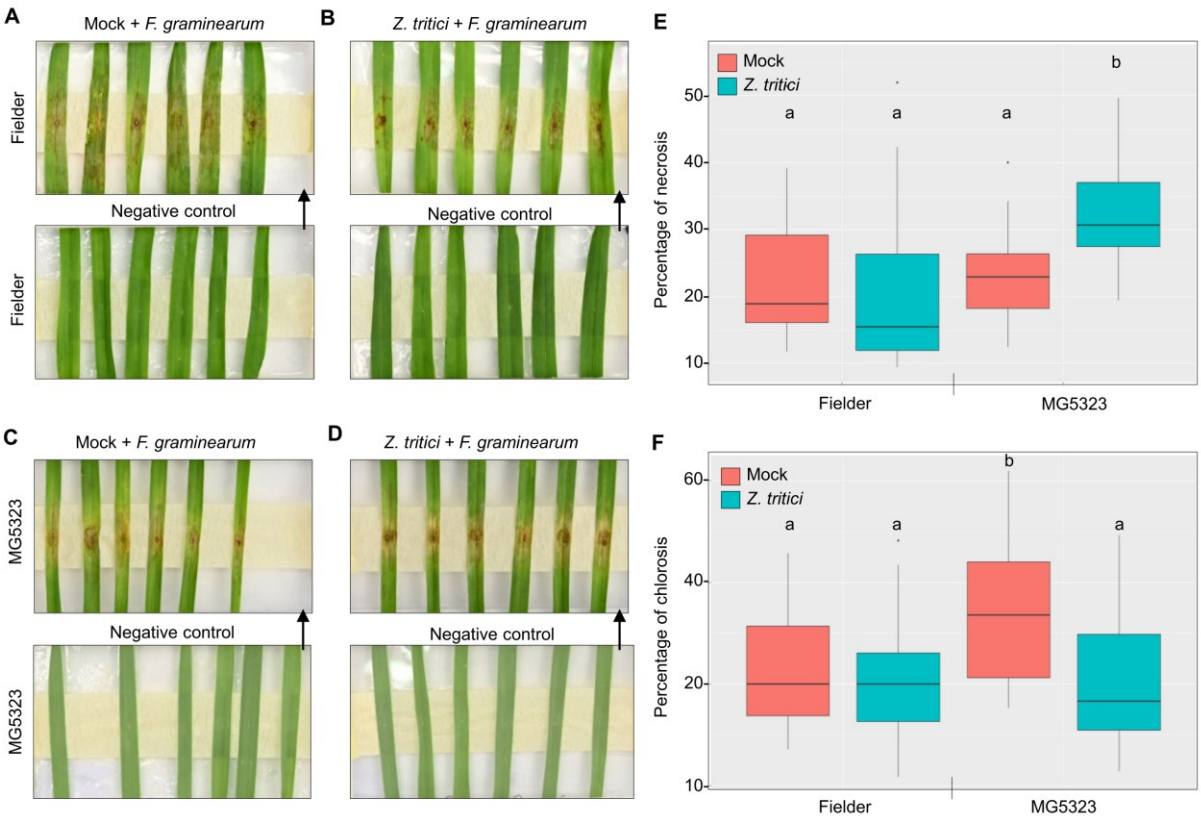

Figure 7. Comparison of *F. graminearum* / *Z. tritici* coinfections of 'Fielder' and 'MG5323'

(A-B) Original pictures from one experiment with 6 biological replicates with the cultivar 'Fielder' applied to our image analysis pipeline. **(A)** Experimental controls for (B) where *Z. tritici* is replaced by Mock (upper panel), and a double negative control where both pathogens are replaced with Mock (lower panel) – both pictures are from the same experiment **(B)** Coinfections with *Z. tritici* and *F. graminearum* (upper panel) and the corresponding double negative control (lower panel). **(C-D)** Original pictures from one experiment with 6 biological replicates with the accession 'MG5323' applied to our image analysis pipeline. **(C)** Experimental controls for (D) as described in (A). **(D)** Coinfections with *Z. tritici* and *F. graminearum* and the corresponding control as described in (B). **(E)** Soring of the percentage necrosis caused on 'Fielder' vs. 'MG5323' where *F. geaminearum* was inoculated alone (red bars) or in combination with *Z. tritici* (blue bars). **(E)** Soring of the percentage chlorosis caused on 'Fielder' vs. 'MG5323' where *F. geaminearum* was inoculated alone (red bars) or in combination with *Z. tritici* (blue bars). The letters a-b refer to two groups of treatments with statistically significant differences (two-way robust ANOVA: $p < 0.05$).